Journal of Colloid and Interface Science 677 (2025) 540–547

Contents lists available at ScienceDirect

Journal of Colloid And Interface Science

journal homepage: www.elsevier.com/locate/jcis

Specific buffer effects on the formation of BSA protein corona around amino-functionalized mesoporous silica nanoparticles

Monica Mura [a,1], Cristina Carucci [a,1], Elena Caddeo [a], Šárka Sovová [b], Marco Piludu [a], Miloslav Pekař [b], Barbara Jachimska [c], Drew F. Parsons [a], Andrea Salis [a,*]

[a] Department of Chemical and Geological Sciences, University of Cagliari &CSGI, Cittadella Universitaria, S.S. 554 bivio Sestu, 09042 Monserrato, CA, Italy
[b] Faculty of Chemistry, Brno University of Technology, Purkynova 464/118, 612 00 Brno, Czechia
[c] Jerzy Haber Institute of Catalysis and Surface Chemistry Polish Academy of Sciences, Krakow, Poland

GRAPHICAL ABSTRACT

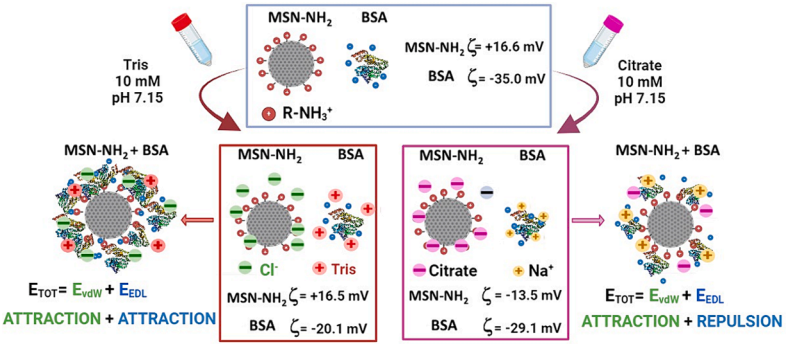

ABSTRACT

The effect of buffer species on biomolecules and biomolecule-nanoparticle interactions is a phenomenon that has been either neglected, or not understood. Here, we study the formation of a BSA protein corona (PC) around amino-functionalized mesoporous silica nanoparticles (MSN-NH_2) in the presence of different buffers (Tris, BES, cacodylate, phosphate, and citrate) at the same pH (7.15) and different concentrations (10, 50, and 100 mM). We find that BSA adsorption is buffer specific, with the adsorbed amount of BSA being 4.4 times higher in the presence of 100 mM Tris (184 ± 3 mg/g) than for 100 mM citrate (42 ± 2 mg/g). That is a considerable difference that cannot be explained by conventional theories. The results become clearer if the interaction energies between BSA and MSN-NH_2, considering the electric double layer (E_{EDL}) and the van der Waals (E_{vdW}) terms, are evaluated. The buffer specific PC derives from buffer specific zeta potentials that, for MSN-NH_2, are positive with Tris and negative with citrate buffers. A reversed sign of zeta potentials can be obtained by considering polarizability-dependent dispersion forces acting together with electrostatics to give the buffer specific outcome. These results are relevant not only to our understanding of the formation of the PC but may also apply to other bio- and nanosystems in biological media.

* Corresponding author.
E-mail address: asalis@unica.it (A. Salis).
[1] MM and CC contributed equally to the work.

https://doi.org/10.1016/j.jcis.2024.07.258
Received 23 April 2024; Received in revised form 13 July 2024; Accepted 31 July 2024
Available online 5 August 2024

1. Introduction

Electrolytes are basic constituents of biological fluids, where they play the fundamental role of modulating the interactions among biomolecules. This role has been only partially understood [1–3]. Biomolecules such as proteins, enzymes, and nucleic acids, carry ionizable groups that, when dissolved in physiological fluids, result in a pH dependent surface charge (Z_p) [4],

$$Z_p = \sum_i \frac{N_i}{1 + 10^{-pK_{ai}+pH+e\psi_0/kT\ln 10}} - \sum_j \frac{N_j}{1 + 10^{pK_{aj}-pH-e\psi_0/kT\ln 10}} \quad (1)$$

where N_i and N_j are the number of basic and acidic amino acid residues having the dissociation constants pK_{ai} and pK_{aj} respectively, e is the elementary charge, ψ_0 is the surface potential, k is the Boltzmann constant, and T is the absolute temperature. Naively, one might be tempted to think Eq. (1) involves only H^+ and OH^- through their determination of pH. But Eq. (1) also involves the surface potential ψ_0, which is influenced by other components of the electrolyte. In living systems, as well as in biochemical labs, the regulation of pH is carried out by mean of buffers, constituted by weak electrolytes in the presence of their conjugated species (e.g. H_2CO_3/HCO_3^-, $H_2PO_4^-/HPO_4^{2-}$, etc.). Thus, once the surface charge has been formed, all the electrolytes (whether strong or weak) interact with charged biointerfaces thus affecting the surface charge/potential. Conventionally, buffer action is considered in terms of the Henderson-Hasselbalch equation ($pH = pK_a + \log([salt]/[base])$) and ion adsorption/screening by the electric double layer (EDL; Stern and Gouy-Chapman) theory [5]. However, conventional theories fail to explain ion specific (Hofmeister) effects [1] observed, for example, in protein aggregation [6], Brownian motion [7], electrophoretic mobility [8]. ion binding to polymers [9]. enzyme activities [10,11], etc. Recent theories [2,12] have successfully rationalised the behaviour of strong electrolytes [13]. Specificity arises through non-electrostatic interactions, such as dispersion forces driven by ion polarizabilities, alongside ion size effects, particularly at high concentrations [2,14]. In some cases, ions may be distinguished by their interaction with the surrounding solvent through their hydration shells [15]. Larger, weakly hydrated ions, known as chaotropes but more recently described using Collins' phrase, "sticky" ions [12,16,17], may readily lose water from their hydration shells. Smaller, strongly hydrated ions (kosmotropes) such as Li^+, Na^+ F^- tend to retain their hydration shell and are less surface active. Ion dispersion forces are often attractive, contributing to stickiness, but in some cases may be repulsive due to the effective polarizability of the hydrated ion in water (via its cavity in the solvent, another size effect) and due to differences in the optical spectra of substrate and solvent. A general specific ion size effect is a "hydrophobic" force pushing larger ions to the interface due to the energy cost of forming the ion hydration cavity [18]. Despite the wealth of studies of specific ion effects in strong electrolytes, the effects of weak electrolytes used as pH buffers have usually been neglected. Indeed, eq. (1) foresees σ_{pH} being affected only by bulk pH and, indirectly, total ionic strength (by screening the magnitude of ψ_0), without considering the chemical nature of the buffer used to regulate pH. However, recent works have shown that buffers play an additional role besides pH regulation and electrostatic screening [19–24]. Pannuru et al. found that the thermal stability of haemoglobin follows the trend Tris-HCl > TES–TAPS [25]. At the same buffer concentration (range 10–100 mM) and pH (=7.15), protein–protein interactions increase specifically with buffer species in the order Tris-H^+ > sodium phosphate > sodium citrate for both bovine serum albumin (BSA) and lysozyme [26]. Lysozyme colloidal stability at fixed pH and ionic strength follows the trend phosphate > HEPES > MOPS > cacodylate [27]. Lysozyme electrophoretic mobility decreases in 10 mM buffer (pH = 7.15) according to the series Tris-H^+ > carbonate > cacodylate > phosphate > citrate.[28] Other examples of buffer specificity include pH measurements [29,30], enzyme activities [31], the interaction of DNA with lipid bilayers [20], etc. Hence, the lack of a general understanding of buffer specific effects poses serious issues to biochemists and biophysicists. For example, it will not be possible to obtain reproducible results among different labs if pH is regulated through different buffers. Proteins dissolved in biological fluids are adsorbed at the surface of nanoparticles used as drug carriers thus altering their physicochemical properties, stability, cell uptake, targeting, pharmacokinetics, biodistribution and cytotoxicity [32]. Adsorbed protein layers around nanoparticles form the so-called "protein corona" (PC) [33]. There are several factors which influence PC formation, including the protein composition of the biofluid [34], nanoparticle features [35], temperature and exposure time [36], pH and ionic strength [37]. Controlled protein adsorption on NPs is an interesting way to regulate the average residence time and efficacy of NPs [38]. Proteins are classified as opsonins and dysopsonins depending on their effect on nanoparticles. The former facilitate endocytosis and clearance by macrophages and other phagocytes [35]. The latter have low affinity for the cell surface and result in a longer residence time of the nanoparticles in the blood stream [39]. Mesoporous silica nanoparticles (MSNs) are widely investigated as carriers for drug delivery purposes [40]. MSNs are often functionalized with amino groups to obtain a positively charged surface at physiological pH (7.1–7.4). Indeed, amine functionalization, to give MSN-NH_2, tends to strengthen electrostatic interactions with bacteria, augmenting the efficacy of the MSNs against infections [41]. Amine functionalization also reduces aggregation, and optimizes adsorption of dysopsonins, such as serum albumins, which have a negative net charge at physiological pH [42].

In this work, we study the specific effect of five commonly used buffers, namely citrate, phosphate, cacodylate, BES and Tris (see chemical structures and dissociation equilibria in Table S3, Supplementary Material), at the same pH 7.15 in a range of concentrations 10–100 mM, on BSA adsorption onto MSN-NH_2 (Scheme 1). We expect that buffers could specifically affect BSA adsorption. Since BSA is a dysopsonin, a layer of this protein might increase the residence time of the drug-loaded nanoparticles in the body. However, the aim of the work goes beyond that. The purpose is in fact to show and understand buffer specificity at nano- and biointerfaces. Only when an updated theory becomes available, can phenomena, like the effect of buffer type and concentration on the formation of the protein corona, be managed.

2. Materials and methods

2.1. Chemicals

Tetraethyl orthosilicate (TEOS 99 %), hexadecyltrimethylammonium bromide (CTAB 99 %), (3-aminopropyl)triethoxysilane (APTES 97 %), sodium citrate dihydrate (99 %), citric acid

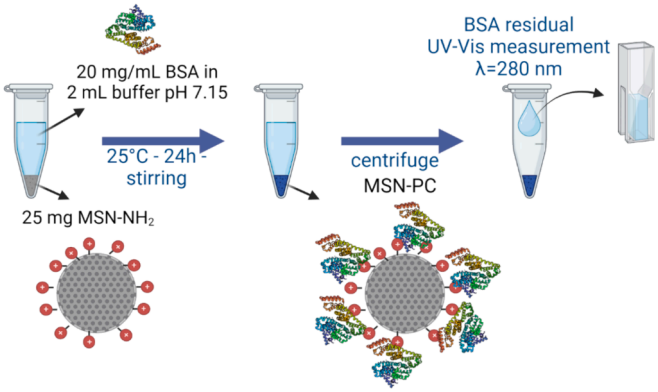

Scheme 1. BSA adsorption on MSN-NH_2. BSA samples are dissolved in different buffers at pH 7.15 to reach a concentration of 20 mg/mL. BSA solution is then added to 25 mg of MSN-NH_2 and left under rotation for 24 h at 25 °C. BSA supernatant is then analyzed through UV-Vis to evaluate the adsorbed amount of BSA on MSN-NH_2.

monohydrate (99 %), monobasic sodium phosphate (99 %), disodium hydrogen phosphate (99 %), cacodylic acid (98 %), hydrochloric acid (37 %), sodium hydroxide (97 %), and bovine serum albumine (BSA) were purchased from Sigma Aldrich. Tris(hydroxymethyl)aminomethane (Tris) was from Bio-Rad (99.8 %). (N,*N*-Bis(2-hydroxyethyl)-2-aminoethanesulfonic acid) (BES-99 %) was purchased from Sigma Life Science. Ammonium nitrate (99 %) was from Carlo Erba; absolute ethanol (99.8 %) was from Honeywall. Water was purified through a Millipore system.

2.2. MSN characterization

MSNs were synthesized and functionalized with APTES prior CTAB removal according to what previously reported [43,44]. MSNs characterization was carried out through a transmission electron microscopy (TEM – JEOL JEM 2010 URP) and small angle x-ray scattering (S3-MICRO SWAX camera system, Hecus X-ray System) having Cu-Kα (λ = 1542 39 Å) X Genix at 30 kV e 0.4 mA. Nitrogen physisorption isotherms at 77 K were acquired through an ASAP 2020 and allowed the measurement of the surface area (S_{BET}) and pore size distribution (d_{BJH}).

Fourier transform infrared spectra (FTIR) of MSN, MSN-NH_2 pre (MSN-T) and post (MSN) CTAB removal were collected by mean of a FTIR-4X JASCO ATR PRO 4X. Thermogravimetric analysis (TGA) was performed within a temperature range 25–850 °C, with a heating rate = 10°C/min, flow rate 50 mL/min, under oxygen flow by means of a Pyris 6 – Perkin Elmer TGA/DSC.

Hydrodynamic size and zeta potential of nanoparticles and BSA were measured by mean of a Zetasizer Nano ZSP (Malvern Instruments) in backscatter configuration for DLS (θ = 173°), at laser wavelength of λ = 633 nm. The samples were prepared in buffer solutions at the concentration of 1 mg mL^{-1} for BSA and of 0.1 mg mL^{-1} for MSN-NH_2, and MSN-NH_2-BSA samples. MSN-NH_2, and MSN-NH_2-BSA samples were dispersed in buffer soltions, sonicated for 15 min until obtaining a suspension without aggregates. Zeta potentials were measured using the Smoluchowski approximation [45].

2.3. BSA adsorption on MSN-NH_2

BSA protein was dissolved in the different buffer solutions (Tris, BES, cacodylate, phosphate, citrate) at different concentrations (10, 50, 100 mM) at the concentration of 20 mg mL^{-1}. Buffer solutions were prepared by dissolving a weighed amount of buffer species (acid and its conjugate base) in an appropriate volume of distilled water to reach a final buffer concentration of 10, 50 and 100 mM. The pH of the buffer solutions was finally adjusted to 7.15 by adding small volumes of either 0.1 M NaOH or HCl solutions. Buffer pH was measured by mean of a Metrohm pHmeter equipped with a combined glass microelectrode (90279010) calibrated using a three-point calibration procedure and standard buffer solutions (pH 4.00, 7.00, and 10.00).

A mass of 25 mg of MSN-NH_2 sample was suspended in a volume of 2 mL of BSA 20 mg mL^{-1}, dissolved in the appropriate buffer (Tris, BES, cacodylate, phosphate, citrate) at pH 7.15 (10, 50, 100 mM) and in water at pH 7.15 into a screw capped glass tube for 24 h at 25 °C. Then, MSNs were centrifuged for 10 min at 4000 rpm. The solid was separated by the supernatant, washed with 1 mL of fresh buffer and re-centrifuged and dried under vacuum at room temperature. The residual concentration of BSA in the supernatant and the washing buffer solutions were obtained by measuring the absorbance at 280 nm through a Cary-60 UV–Vis spectrophotometer in a quartz cuvette with a dilution factor of 1:40. BSA exact concentrations were determined through BSA calibration curves in each buffer 10, 50 and 100 mM with a protein concentration range 0.1–1 mg mL^{-1}. The adsorbed amount of BSA ($A.A._{BSA}$; mg/g) was determined according to:

$$A.A._{BSA} = \frac{([BSA]_0 - [BSA]_{eq.}) \times V}{m_{MSN-NH2}}$$

where $[BSA]_0$ and $[BSA]_{eq.}$ are the initial and equilibrium concentrations of BSA, respectively. V is the volume of BSA solution and $m_{MSN-NH2}$ is the mass (g) of functionalized mesoporous silica nanoparticles (MSN-NH_2).

3. Results and discussion

TEM images (Fig. 1A,B) of MSNs show particles of quasi-spherical shape with a size around 150–180 nm and a hexagonal array of pores, confirmed by the 100, 110, and 200 peaks of SAXS analysis (Fig. 1C). Nitrogen adsorption/desorption isotherms (Fig. 1D) allowed the determination of a surface area of 675 m^2 g^{-1} (Table S1). Additional characterizations, e.g. FTIR spectroscopy and thermogravimetric analysis, are reported in Fig. S1 (Supplementary material) whereas hydrodynamic size (d_H) and the zeta potential (ζ) in MilliQ water are listed in Table S2.

Fig. 2 shows the effect of buffer type and concentration, in the range 10–100 mM, on BSA adsorption on MSN-NH_2 at the same pH = 7.15. The adsorbed amount of BSA decreases with increasing buffer concentration (10 mM > 50 mM > 100 mM) for anionic buffers (cacodylate, phosphate, and citrate). Zwitterionic BES buffer, which has a slight excess of negative charges at pH 7.15 (pK_a = 7.09) presents a decrease of BSA adsorption going from 10 to 50 mM and remains unchanged at 100 mM. In contrast, the cationic Tris-H^+ buffer results in a slight increasing amount of adsorbed BSA as buffer concentration increases (10 mM < 50 mM < 100 mM). The results in Fig. 2 clearly show that, even at the same pH (7.15), the different buffers affect specifically the adsorption of BSA on MSN-NH_2 surface which, at the same concentration (i.e. 100 mM), decreases along the series Tris (184 ± 3 mg g^{-1}) > BES (124 ± 3 mg g^{-1}) > cacodylate (87 ± 3 mg g^{-1}) > phosphate (53 ± 1 mg g^{-1}) > citrate (42 ± 2 mg g^{-1}).

A possible way to explain the trends in Fig. 2 is to consider the interactions involved on protein adsorption on charged surfaces. In a simple model, the total interaction energy E_{TOT} between BSA molecules and MSN-NH_2 surface is given by,

$$E_{TOT} = E_{vdW} + E_{EDL} \quad (2)$$

where E_{vdW} is the energy due to van der Waals forces (dominated by dispersion forces) and depends on the Hamaker constant. E_{EDL} is an interaction energy associated with the overlapping of the electric double layers of the BSA protein and that of MSN-NH_2 particles. We expect that the first contribution is attractive due to a positive value of the Hamaker constant (*A*) that depends on the optical (*n*, refractive index) and dielectric (ε, permittivity) properties of the involved materials/media (silica, water, and protein). E_{vdW} is not affected by buffers and for spherical particles, of radii R_1 and R_2 at a distance *D*, is given by [46],

$$E_{vdW} = \frac{-A}{6D} \times \frac{R_1 R_2}{R_1 + R_2} \quad (3)$$

The double-layer energy (E_{EDL}), for spherical particles of radii R_1 and R_2 at a distance *D*, can be approximately estimated from the adsorption of electrolyte ions by the expression [47],

$$E_{EDL} = \frac{\pi \varepsilon_0 \varepsilon_r R_1 R_2 (\psi_1^2 + \psi_2^2)}{R_1 + R_2} \times \left\{ \frac{2\psi_1\psi_2}{\psi_1^2 + \psi_2^2} \times \ln \frac{1 + \exp(-\kappa D)}{1 - \exp(-\kappa D)} + \ln[1 - \exp(-2\kappa D)] \right\} \quad (4)$$

where ε_0 and ε_r are the permittivity of vacuum and the relative permittivity, respectively; ψ_1 and ψ_2 are the surface potentials of isolated particles of BSA and MSN-NH_2, respectively; κ is the inverse of the Debye length for each buffer solution, calculated by:

$$\kappa = \left(\frac{2e^2 I}{\varepsilon_0 \varepsilon_r k_B T} \right)^{\frac{1}{2}} \quad (5)$$

Table 1 shows that buffers at the same concentration result in a

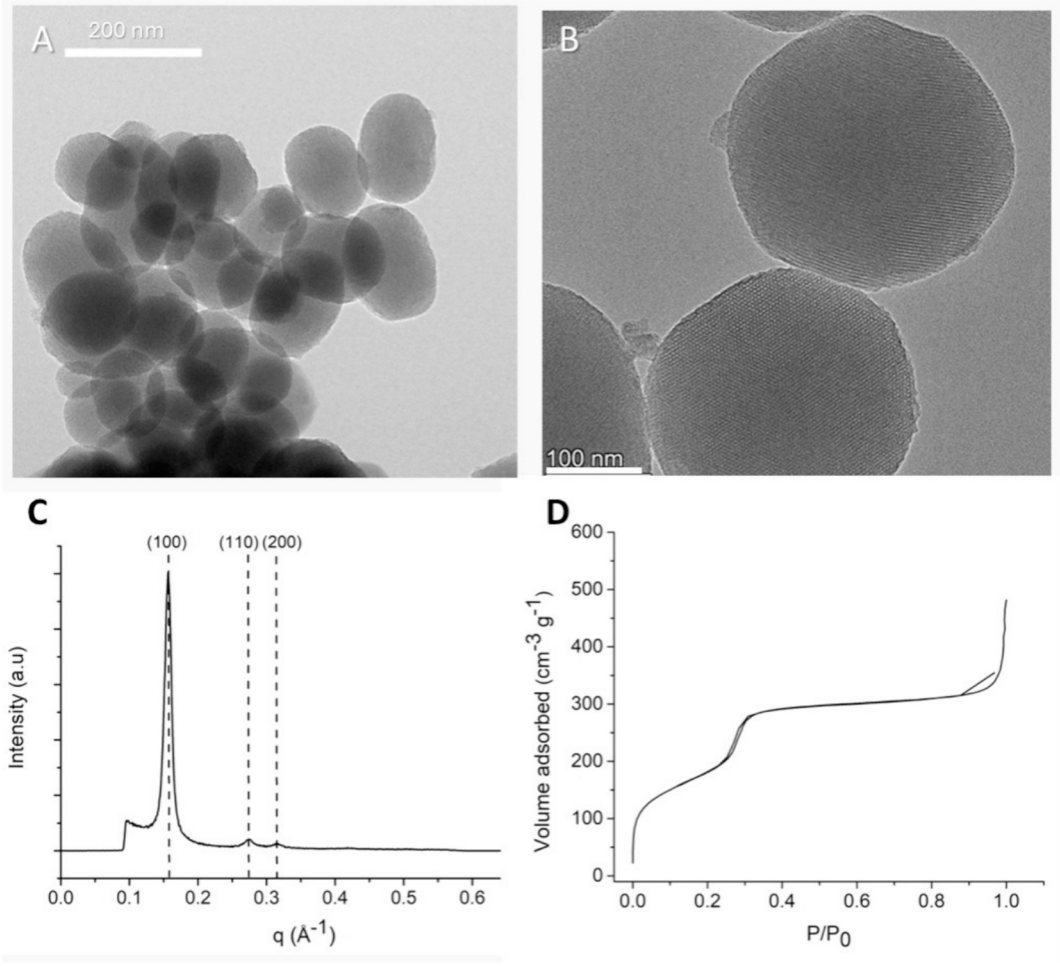

Fig. 1. Structural characterization of MSN-NH_2. Transmission electron microscopy images at two different magnifications (A–B), SAXS pattern (C) and adsorption/desorption N_2 isotherms (D).

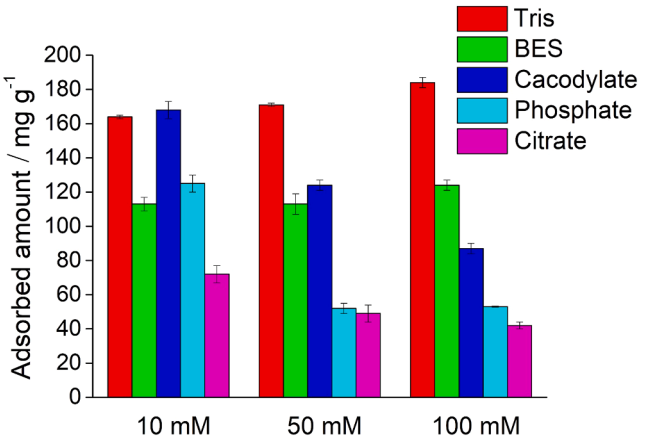

Fig. 2. Specific buffer effects on BSA adsorption on MSN-NH_2 at pH 7.15, T = 25 °C. Buffer concentrations of 10 mM, 50 mM and 100 mM. Each experiment was repeated from 3 to 5 times, and the results are presented as the mean ± standard deviation.

different ionic strength ($I = \frac{1}{2}\sum_i c_i z_i^2$), due to the different concentrations (c_i) and charges (z_i) of the buffer species, resulting in different Debye lengths. Hence, according to eq. (4), E_{EDL} would specifically be affected by buffer type through Debye lengths.

Moreover, the calculation of E_{EDL} requires the surface potentials of

Table 1
Ionic strength and Debye length for buffer solutions at different concentrations (10, 50, and 100 mM).

Buffer	Ionic strength (I/mM)			Debye length (κ^{-1}/nm)		
	10 mM	50 mM	100 mM	10 mM	50 mM	100 mM
Tris	8.9	44.5	89.1	3.2	1.4	1.0
BES	5.4	26.7	53.5	4.2	1.9	1.3
Cacodylate	8.8	43.8	87.6	3.2	1.5	1.0
Phosphate	19.2	84.5	192.0	2.2	1.0	0.7
Citrate	54.0	270	540	1.3	0.6	0.4

BSA and MSN-NH_2 (ψ_1 and ψ_2) to be estimated. This has been done by measuring zeta potentials through electrophoretic light scattering (ELS). The experimental zeta potential of BSA (ζ_1 and MSN-NH_2 (ζ_2), shown in Fig. 3, are the result of the screening of $\psi_{0,1}$ and $\psi_{0,2}$ (with ψ_0 we mean the surface potential, that is at x = 0 nm from the surface) due to buffer ion adsorption within the slipping plane. At pH 7.15 and in the absence of buffers, BSA has a net negative charge due to a higher number of negative carboxylate groups than positive amine groups (isoelectric point, pI ≈ 4.7) [48] with a $\zeta_1 = -23.3mV$. In the presence of buffers, at the same pH (7.15), we observe a less negative zeta potential with increasing buffer concentration due to counterion (cation) adsorption (Fig. 3A).

However, the BSA zeta potential is buffer specific increasing in absolute value along the series Tris < BES < cacodylate < citrate < phosphate. This trend can be understood if we consider that, alongside

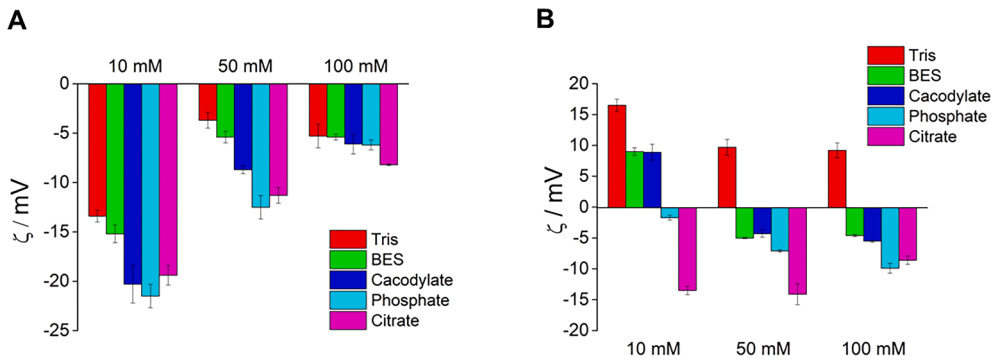

Fig. 3. Zeta potential measurements of (A) BSA and (B) MSN-NH_2 at buffer concentration of 10 mM, 50 mM and 100 mM. Each experiment was repeated from 3 to 5 times, and the results are presented as the mean ± standard deviation.

the adsorption of counterions (cations, either Tris-H^+ or Na^+), anionic buffer species (cacodylate, phosphate, citrate) are also adsorbed on the BSA surface, likely at the residual positive sites or at neutral patches by mean of nonelectrostatic dispersion forces [7]. The impact of such nonelectrostatic interactions on the zeta potentials is distinct from the electrostatic screening of carboxylates by cationic counterions; cation screening decreases the (negative) magnitude of the BSA zeta potential, anion adsorption increases it. A similar buffer specific trend was found in the BSA diffusion coefficient, which decreased according to the series Tris-H^+ > phosphate > citrate [26]. Fig. 3B shows the values of MSN-NH_2 zeta potentials in the presence of 10, 50, and 100 mM buffers all at pH 7.15. At the same pH, but in the absence of buffers, MSN-NH_2 is positively charged with $\zeta_2 = +16.6mV$ due to the protonation of the amine groups (pI ≈ 8). In the presence of buffers, the zeta potential of MSN-NH_2 is different depending on the buffer type and concentration. At a buffer concentration of 10 mM, ζ_2 is positive for Tris, BES and cacodylate but becomes slightly negative for phosphate (−1.7 mV) and more negative for citrate (−13.5 mV). Moreover, at 50 mM and 100 mM zeta potential remains positive only for Tris, whereas all the other buffers result in a negative zeta potential. This is a relevant result previously observed for lysozyme protein [49]. In general, MSN-NH_2 zeta potential decreases in the order Tris > BES > cacodylate > phosphate > citrate, following the same sequence found with BSA adsorption (see Fig. 2).

Zeta potential measurements of MSN-NH_2-BSA samples, following the 24-hour long incubation step, were carried out as control experiments to confirm the formation of the BSA corona around MSN-NH_2. Measurements were both carried out in buffers (Fig. 4A) and in MilliQ water (Fig. 4B) after adjusting pH at 7.15. Zeta potentials of MSN-NH_2-BSA samples are all negative, confirming the formation of the protein corona, since BSA is negatively charged at pH 7.15 (Fig. 3A). Then, we also observe a clear specific buffer effect of zeta potentials carried out in buffer solutions (see for example data at 10 mM) and, in general, the trend in Fig. 4A for the adsorbed BSA on MSN-NH_2 (protein corona) is very similar to that of dissolved BSA in Fig. 3A. This confirms that buffer species are adsorbed within the slipping plane. Zeta potential measurements of MSN-NH_2-BSA samples in MilliQ water (Fig. 4B) are all negative, confirming the formation of protein corona but, as expected, they are all similar (about −35 mV) due to the use of water as the dispersing medium instead of the buffers.

Similarly to the buffer-specific variations in BSA zeta potential, the observed phenomenon of the inversion of the MSN-NH_2 zeta potential, known as "charge reversal", cannot be explained with electrostatics. Indeed, if buffer ions were interacting with MSN-NH_2 surface through electrostatic interactions alone, at most the neutralization of the surface charge would be expected. The phenomenon of charge reversal can be explained through the action of additional ion dispersion forces [50]. Dispersion forces depend on the temporary fluctuations in electron distribution of ions and molecules. These fluctuations affect the surroundings, causing a similar distribution in other ion/molecules. This transient interaction between temporary charge distributions creates an attractive force between ion and surfaces. The key parameter of these interactions is the polarizability. Polarizabilities are ion-specific physico-chemical parameters [51]. The dispersion interaction can be included in the Poisson-Boltzmann equation by an additional term μ_{disp} [50],

$$\frac{d^2\psi}{dx^2} = -\sum_i \frac{z_i e n_{i0}}{\varepsilon_0 \varepsilon_w} e^{-\frac{z_i e\psi(x)+\mu_{disp}}{kT}} \quad (6)$$

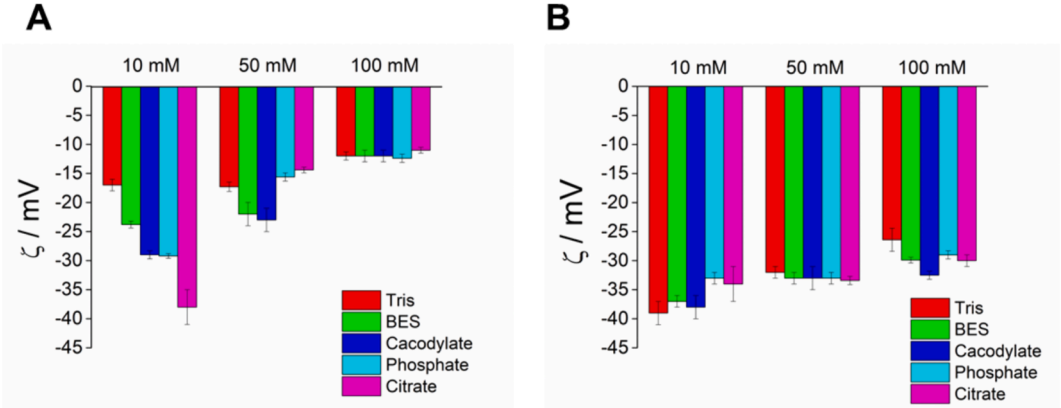

Fig. 4. Zeta potential measurements of the BSA corona adsorbed onto the MSN-NH_2, following the 24-hour long incubation step in (A) different buffers all at pH = 7.15 and different concentrations and in (B) MilliQ water with the adjusted pH at 7.15. Each experiment was repeated from 3 to 5 times, and the results are presented as the mean ± standard deviation.

Once we have understood that buffer species interact specifically through both electrostatic and dispersion forces with both BSA and MSN-NH_2 surfaces modulating their zeta potentials, we have all the tools in our hands to explain the trends in the adsorbed amount observed in Fig. 2, by calculating interaction energies with the help of Eqs. (2)–(5). We first calculate the E_{EDL} term by using the buffer specific values of zeta potentials (Fig. 5A) in Eq. (4). At all concentrations the E_{EDL} term is buffer specific, although at 10 mM, it is attractive for Tris, BES, cacodylate and phosphate and repulsive for citrate. At 50 and 100 mM, on the other hand, E_{EDL} is attractive only for Tris and repulsive for all the other buffers. That is a surprising result since common wisdom would have suggested an attractive electrostatic interaction between MSN-NH_2 and BSA at pH 7.15 regardless of the buffer used to obtain it.

This is indeed due to the charge reversal of MSN-NH_2 obtained via specific adsorption of buffer species. However, if E_{EDL} was the only interaction energy at work, we should not have BSA adsorption onto MSN-NH_2 in the presence of anionic buffers at 50 and 100 mM. In fact, in these cases adsorption is driven by the van der Waals energy. Using a Hamaker constant, A = 1.448 kT [52], and the distance (D) of 1 nm, we can use Eq. (3) to calculate the van der Waals energy obtaining $E_{vdW} = -3.4 \times 10^{-21}$ J. This term is constant and not affected by buffers. Fig. 5B shows the total interaction energy between the BSA and the MSN-NH_2 calculated through Eq. (2). Interestingly, E_{TOT} shows a trend like that seen in the buffer specificity of the BSA adsorption data (Fig. 2). We remark that adsorbed amounts (Fig. 2) and interaction energies (Fig. 5) were obtained through different experimental techniques, that is UV–visible spectroscopy and electrophoretic light scattering (for the experimental determination of zeta potentials), respectively. These independent techniques lead us to observe a similar buffer specific trend. The more negative the energy, the stronger the interaction, which results in a higher adsorbed amount of BSA.

Fig. 6A and show the contributions of E_{EDL} and E_{vdW} as a function of the distance for 10 mM Tris and citrate buffers. Both E_{EDL} and E_{vdW} are negative (attractive interaction) for Tris, whereas E_{EDL} is positive (repulsive interaction) for citrate. These differences in E_{EDL} values provide the origin of the buffer specific trend observed for both the calculated E_{TOT} (Fig. 6C) and the experimentally measured BSA adsorption (Fig. 2).

4. Conclusions

In summary, the present study shows that protein adsorption on nanoparticles at physiological pH is buffer-specific. To demonstrate it, we carried out adsorption of BSA protein onto MSN-NH_2 in different buffers at three different concentrations but all at the same pH (7.15). The chosen buffers are commonly used to simulate physiological fluids with little or no awareness of their specific effects. BSA loading, at 100 mM buffer concentration, decreases in the order Tris > BES > cacodylate > phosphate > citrate. Buffer effects have seldom been considered, and if observed not understood [24,53,54]. Moreover, the impact of buffers on protein-NP interactions was not previously investigated. To promote the formation of a dysopsonin (i.e. BSA) protein corona on MSN-NH_2, Tris buffer is more suitable than citrate. To better understand the causes behind the specificity, we studied how buffers affect the zeta potential of proteins and nanoparticles. The buffer specificity is the result of two effects, one due to ionic strength which affects the Debye length, that is of electrostatic nature. The other is due to ion dispersion forces that lead to charge reversal, seen in the zeta potentials of MSN-NH_2. The latter is the dominating effect and should be considered the true phenomenon responsible for buffer specificity. Zeta potentials have been used to calculate BSA/MSN-NH_2 interaction energies with conventional equations of E_{EDL} and E_{vdW}. The obtained E_{TOT}, clearly shows buffer specificity and follows a similar trend of BSA adsorption data. A new theory, based on the inclusion of ion dispersion forces, has been able to predict buffer specific zeta potentials for lysozyme protein [28]. The same approach will be used to predict zeta potentials and interaction energies for the formation of the protein corona. The composition of the used buffers is, of course, simpler than the composition of the body fluids which nanoparticles could encounter in living organisms. The ion effects on the protein corona formation in real environments can thus be more intricate. Nevertheless, experimental studies on nanoparticles for medical purposes are often realized in a single buffer or aqueous environment. This study points out that results of such studies cannot be directly transferable to more complex fluids, at least from the point of protein corona forming which is an inevitable process when introducing nanoparticles into the human body.

Author contributions

The manuscript was written through contributions of all authors. All authors have given approval to the final version of the manuscript.

CRediT authorship contribution statement

Monica Mura: Writing – original draft, Investigation, Data curation. **Cristina Carucci:** Writing – original draft, Methodology, Investigation, Conceptualization. **Elena Caddeo:** Investigation, Data curation. **Šárka Sovová:** Investigation, Data curation. **Marco Piludu:** Investigation, Data curation. **Miloslav Pekař:** Writing – original draft. **Barbara Jachimska:** Writing – original draft, Funding acquisition. **Drew F. Parsons:** Writing – original draft, Validation, Conceptualization. **Andrea Salis:** Writing – original draft, Supervision, Funding acquisition, Formal analysis, Data curation, Conceptualization.

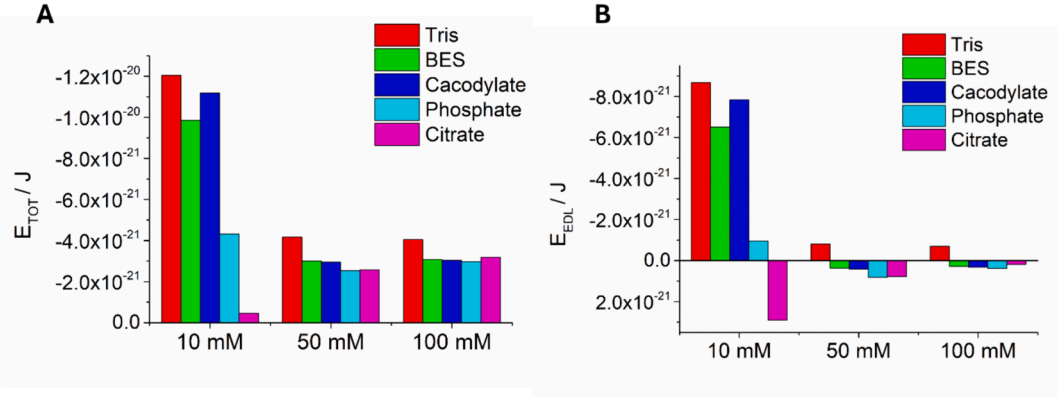

Fig. 5. Specific buffer effects on energy interaction between BSA and MSN-NH_2 at an interaction distance of 1 nm. Electric double layer energy (A); total energy (E_{EDL} + E_{vdW}) (B). NB: the y axis in both A and B is reversed (negative values) for an easier comparison with Fig. 2.

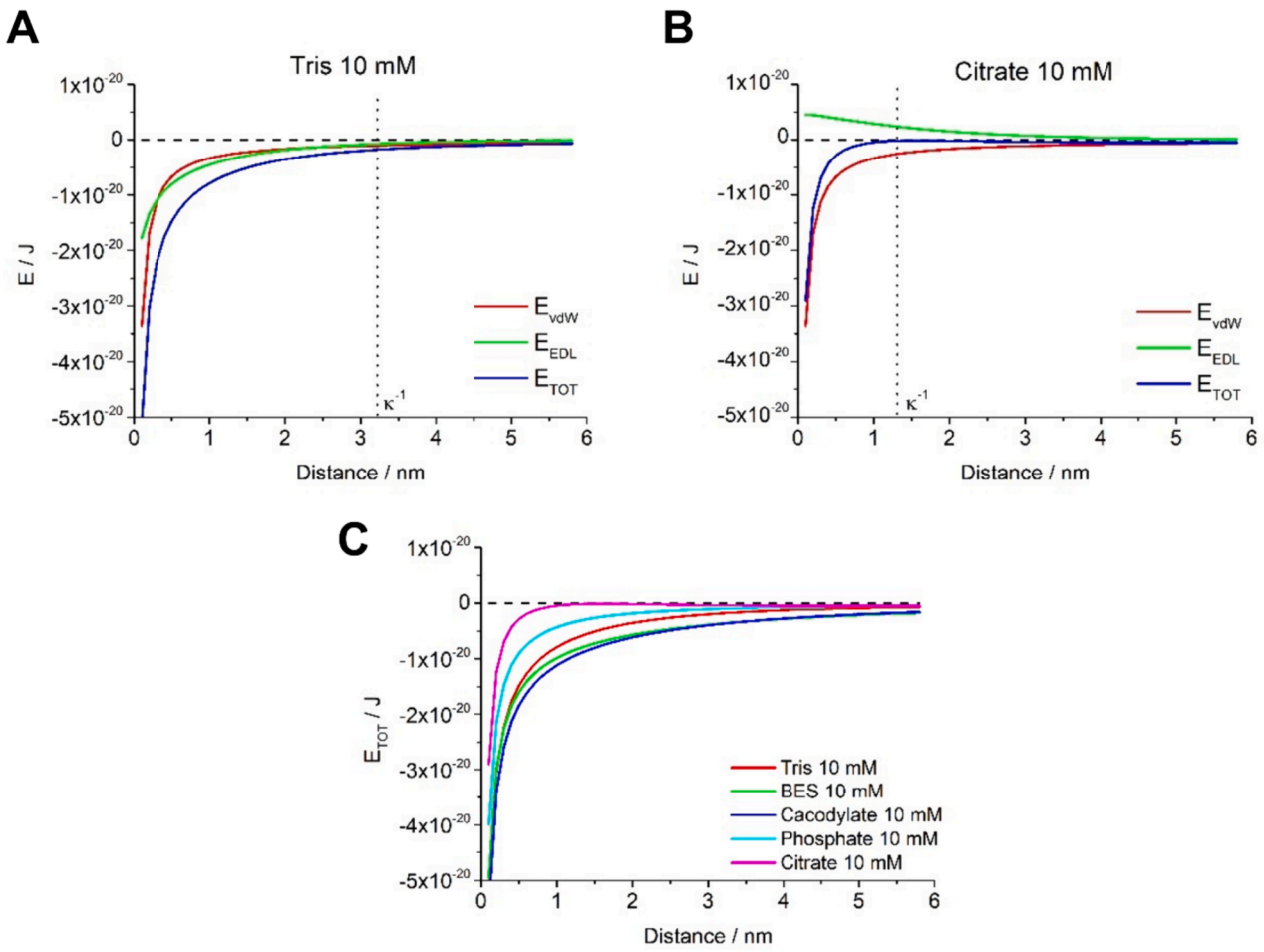

Fig. 6. Interaction energies between BSA and MSN-NH_2 vs distance for 10 mM buffer concentration. (A) van der Waals energy (E_{vdW}: red line), electric double layer energy (E_{EDL}: green line) and total energy (E_{TOT}: blue line) are reported for 10 mM Tris buffer (B) and 10 mM citrate buffer. (C). Specific buffer effect on total interaction energy (E_{TOT}). All plots for different buffers at different concentrations are reported in Supplementary material (Figs. S3–S5). (For interpretation of the references to colour in this figure legend, the reader is referred to the web version of this article.)

Declaration of competing interest

The authors declare that they have no known competing financial interests or personal relationships that could have appeared to influence the work reported in this paper.

Data availability

Data will be made available on request.

Acknowledgment

The present work was funded by Canaletto Program Italy-Poland 2022-2023 (MAECI, PO22MO04 and NAWA, PPN/BIT/2021/1/0008). SS thanks and ACRI for Young Investigator Training Program (YITP) 2019 for funding her research period at the University of Cagliari. AS and CC thank Fondazione di Sardegna (F72F20000230007) and CSGI for funding. The instrumentation centre CeSAR (Centro Servizi di Ateneo per la Ricerca) of the University of Cagliari, Italy, is acknowledged for access to a JEM 1400 Plus TEM microscope.

Appendix A. Supplementary material

Supplementary data to this article can be found online at https://doi.org/10.1016/j.jcis.2024.07.258.

References

[1] P. Lo Nostro, B.W. Ninham, Hofmeister phenomena: an update on ion specificity in biology, Chem. Rev. 112 (2012) 2286–2322, https://doi.org/10.1021/cr200271j.
[2] K.P. Gregory, G.R. Elliott, H. Robertson, A. Kumar, E.J. Wanless, G.B. Webber, V.S. J. Craig, G.G. Andersson, A.J. Page, Understanding specific ion effects and the Hofmeister series, Phys. Chem. Chem. Phys. 24 (2022) 12682–12718, https://doi.org/10.1039/d2cp00847e.
[3] C. Duan, R. Wang, A unified description of salt effects on the liquid-liquid phase separation of proteins, ACS Cent. Sci. 10 (2024) 460–468, https://doi.org/10.1021/acscentsci.3c01372.
[4] B. Mörnstam, K.-G. Wahlund, B. Jönsson, Potentiometric acid−base titration of a colloidal solution, Anal. Chem. 69 (1997) 5037–5044, https://doi.org/10.1021/ac970451a.
[5] M.A. Brown, G.V. Bossa, S. May, Emergence of a stern layer from the incorporation of hydration interactions into the Gouy-Chapman model of the electrical double layer, Langmuir. 31 (2015) 11477–11483, https://doi.org/10.1021/acs.langmuir.5b02389.
[6] D.F. Parsons, T.T. Duignan, A. Salis, Cation effects on haemoglobin aggregation: balance of chemisorption against physisorption of ions, Interface Focus. 7 (2017) 20160137, https://doi.org/10.1098/rsfs.2016.0137.
[7] L. Medda, M. Monduzzi, A. Salis, The molecular motion of bovine serum albumin under physiological conditions is ion specific, Chem. Commun. 51 (2015) 6663–6666, https://doi.org/10.1039/c5cc01538c.
[8] L. Medda, B. Barse, F. Cugia, M. Boström, D.F. Parsons, B.W. Ninham, M. Monduzzi, A. Salis, Hofmeister challenges: ion binding and charge of the BSA protein as explicit examples, Langmuir. 28 (2012) 16355–16363, https://doi.org/10.1021/la3035984.
[9] B.A. Rogers, H.I. Okur, C. Yan, T. Yang, J. Heyda, P.S. Cremer, Weakly hydrated anions bind to polymers but not monomers in aqueous solutions, Nat. Chem. 14 (2022) 40–45, https://doi.org/10.1038/s41557-021-00805-z.

[10] M. Acar, D. Tatini, M.A. Budroni, B.W. Ninham, M. Rustici, F. Rossi, P. Lo Nostro, Specific anion effects on urease activity: a Hofmeister study, Colloids Surf. B Biointerf. 236 (2024) 113789, https://doi.org/10.1016/j.colsurfb.2024.113789.
[11] C. Carucci, F. Raccis, A. Salis, E. Magner, Specific ion effects on the enzymatic activity of alcohol dehydrogenase from Saccharomyces cerevisiae, Phys. Chem. Chem. Phys. 22 (2020) 6749–6754, https://doi.org/10.1039/C9CP06800G.
[12] E. Leontidis, Investigations of the Hofmeister series and other specific ion effects using lipid model systems, Adv. Colloid Interface Sci. 243 (2017) 8–22, https://doi.org/10.1016/j.cis.2017.04.001.
[13] D.F. Parsons, M. Boström, P. Lo Nostro, B.W. Ninham, Hofmeister effects: interplay of hydration, nonelectrostatic potentials, and ion size, Phys. Chem. Chem. Phys. 13 (2011) 12352–12367, https://doi.org/10.1039/c1cp20538b.
[14] R.I. Slavchov, J.K. Novev, Surface tension of concentrated electrolyte solutions, J. Colloid Interface Sci. 387 (2012) 234–243, https://doi.org/10.1016/j.jcis.2012.07.020.
[15] K.D. Collins, Charge Density-Dependent Strength, Biophys. J. 72 (1997) 65–76. https://www.sciencedirect.com/science/article/pii/S0006349597786478.
[16] K.D. Collins, Sticky ions in biological systems, Proc. Natl. Acad. Sci. U.S.A. 92 (1995) 5553–5557, https://doi.org/10.1073/pnas.92.12.5553.
[17] B. Peychev, R.I. Slavchov, Interactions between Small Inorganic Ions and Uncharged Monolayers on the Water/Air Interface, J. Phys. Chem. B. 127 (2023) 2801–2817, https://doi.org/10.1021/acs.jpcb.2c08019.
[18] T.T. Duignan, D.F. Parsons, B.W. Ninham, Ion interactions with the air-water interface using a continuum solvent model, J. Phys. Chem. B. 118 (2014) 8700–8710, https://doi.org/10.1021/jp502887e.
[19] M. Mura, C. Carucci, F.C. Marincola, M. Monduzzi, D.F. Parsons, A. Salis, The melting curves of calf thymus-DNA are buffer specific, J. Colloid Interface Sci. 630 (2023) 193–201, https://doi.org/10.1016/j.jcis.2022.10.018.
[20] M. Mura, B. Humphreys, J. Gilbert, A. Salis, T. Nylander, Cation and buffer specific effects on the DNA-lipid interaction, Colloids Surf. B Biointerf. 223 (2023) 113187, https://doi.org/10.1016/j.colsurfb.2023.113187.
[21] K. Krollik, A. Lehmann, C. Wagner, J. Kaidas, H. Kubas, W. Weitschies, The effect of buffer species on biorelevant dissolution and precipitation assays – comparison of phosphate and bicarbonate buffer, Eur. J. Pharm. Biopharm. 171 (2022) 90–101, https://doi.org/10.1016/j.ejpb.2021.09.009.
[22] M.M. Koerner, L.A. Palacio, J.W. Wright, K.S. Schweitzer, B.D. Ray, H.I. Petrache, Electrodynamics of lipid membrane interactions in the presence of zwitterionic buffers, Biophys. J. 101 (2011) 362–369, https://doi.org/10.1016/j.bpj.2011.05.062.
[23] J.R. Wenner, V.A. Bloomfield, Buffer effects onEcoRV kinetics as measured by fluorescent staining and digital imaging of plasmid cleavage, Anal. Biochem. 268 (1999) 201–212, https://doi.org/10.1006/abio.1998.3079.
[24] A. Salis, M. Monduzzi, Not only pH. Specific buffer effects in biological systems, Curr. Opin. Colloid Interface Sci. 23 (2016) 1–9, https://doi.org/10.1016/j.cocis.2016.04.004.
[25] P. Pannuru, B.S. Gupta, J. Cherng, H. Ming, J. Lee, Biomolecular interactions of selected buffers with hemoglobin, J. Therm. Anal. Calorim. 142 (2020) 2003–2013. https://doi.org/10.1007/s10973-020-09947-7.
[26] A. Salis, L. Cappai, C. Carucci, D.F. Parsons, M. Monduzzi, Specific buffer effects on the intermolecular interactions among protein molecules at physiological pH, J. Phys. Chem. Lett. 11 (2020) 6805–6811, https://doi.org/10.1021/acs.jpclett.0c01900.
[27] S. Brudar, B. Hribar-Lee, Effect of buffer on protein stability in aqueous solutions: a simple protein aggregation model, J. Phys. Chem. B. 125 (2021) 2504–2512, https://doi.org/10.1021/acs.jpcb.0c10339.
[28] F. Cugia, M. Monduzzi, B.W. Ninham, A. Salis, Interplay of ion specificity, pH and buffers: Insights from electrophoretic mobility and pH measurements of lysozyme solutions, RSC Adv. 3 (2013) 5882–5888, https://doi.org/10.1039/c3ra00063j.
[29] A.E. Voinescu, P. Bauduin, M.C. Pinna, D. Touraud, B.W. Ninham, W. Kunz, Similarity of salt influences on the pH of buffers, polyelectrolytes, and proteins, J. Phys. Chem. B. 110 (2006) 8870–8876, https://doi.org/10.1021/jp0600209.
[30] A. Salis, M.C. Pinna, D. Bilaničová, M. Monduzzi, P. Lo Nostro, B.W. Ninham, Specific anion effects on glass electrode pH measurements of buffer solutions: bulk and surface phenomena, J. Phys. Chem. B. 110 (2006) 2949–2956, https://doi.org/10.1021/jp0546296.
[31] H. Kim, E. Tuite, B. Norden, B.W. Ninham, Co-ion dependence of DNA nuclease activity suggests hydrophobic cavitation as a potential source of activation energy, Eur. Phys. J. E. 4 (2001) 411–417.
[32] Q. Xiao, M. Zoulikha, M. Qiu, C. Teng, C. Lin, X. Li, M.A. Sallam, Q. Xu, W. He, The effects of protein corona on in vivo fate of nanocarriers, Adv. Drug Deliv. Rev. 186 (2022) 114356, https://doi.org/10.1016/j.addr.2022.114356.
[33] M. Mahmoudi, M.P. Landry, A. Moore, R. Coreas, The protein corona from nanomedicine to environmental science, Nat. Rev. Mater. 8 (2023) 422–438, https://doi.org/10.1038/s41578-023-00552-2.
[34] A.E. Nel, L. Mädler, D. Velegol, T. Xia, E.M.V. Hoek, P. Somasundaran, F. Klaessig, V. Castranova, M. Thompson, Understanding biophysicochemical interactions at the nano-bio interface, Nat. Mater. 8 (2009) 543–557, https://doi.org/10.1038/nmat2442.
[35] M. Mahmoudi, I. Lynch, M.R. Ejtehadi, M.P. Monopoli, F.B. Bombelli, S. Laurent, Protein-nanoparticle interactions: opportunities and challenges, Chem. Rev. 111 (2011) 5610–5637, https://doi.org/10.1021/cr100440g.
[36] R.K. Mishra, A. Ahmad, A. Vyawahare, P. Alam, T.H. Khan, R. Khan, Biological effects of formation of protein corona onto nanoparticles, Int. J. Biol. Macromol. 175 (2021) 1–18, https://doi.org/10.1016/j.ijbiomac.2021.01.152.
[37] A.V. Bychkova, M.V. Lopukhova, L.A. Wasserman, Y.N. Degtyarev, A.L. Kovarski, S. Chakraborti, V.A. Mitkevich, The influence of pH and ionic strength on the interactions between human serum albumin and magnetic iron oxide nanoparticles, Int. J. Biol. Macromol. 194 (2022) 654–665, https://doi.org/10.1016/j.ijbiomac.2021.11.110.
[38] T. Kopac, Protein corona, understanding the nanoparticle–protein interactions and future perspectives: a critical review, Int. J. Biol. Macromol. 169 (2021) 290–301, https://doi.org/10.1016/j.ijbiomac.2020.12.108.
[39] E. Papini, R. Tavano, F. Mancin, Opsonins and dysopsonins of nanoparticles: facts, concepts, and methodological guidelines, Front. Immunol. 11 (2020) 1–19, https://doi.org/10.3389/fimmu.2020.567365.
[40] M. Vallet-Regí, F. Schüth, D. Lozano, M. Colilla, M. Manzano, Engineering mesoporous silica nanoparticles for drug delivery: where are we after two decades? Chem. Soc. Rev. 51 (2022) 5365–5451, https://doi.org/10.1039/d1cs00659b.
[41] A. Aguilar-Colomer, M. Colilla, I. Izquierdo-Barba, C. Jiménez-Jiménez, I. Mahillo, J. Esteban, M. Vallet-Regí, Impact of the antibiotic-cargo from MSNs on gram-positive and gram-negative bacterial biofilms, Micropor. Mesopor. Mater. 311 (2021), https://doi.org/10.1016/j.micromeso.2020.110681.
[42] B.M. Estevão, I. Miletto, N. Hioka, L. Marchese, E. Gianotti, Mesoporous silica nanoparticles functionalized with amino groups for biomedical applications, ChemistryOpen. 10 (2021) 1251–1259, https://doi.org/10.1002/open.202100227.
[43] V. Nairi, L. Medda, M. Monduzzi, A. Salis, Adsorption and release of ampicillin antibiotic from ordered mesoporous silica, J. Colloid Interface Sci. 497 (2017) 217–225, https://doi.org/10.1016/j.jcis.2017.03.021.
[44] C. Carucci, G. Sechi, M. Piludu, M. Monduzzi, A. Salis, A drug delivery system based on poly-L-lysine grafted mesoporous silica nanoparticles for quercetin release, Colloids Surf. A Physicochem. Eng. Asp. 648 (2022) 129343, https://doi.org/10.1016/j.colsurfa.2022.129343.
[45] T.L. Doane, C.H. Chuang, R.J. Hill, C. Burda, Nanoparticle ζ -potentials, Acc. Chem. Res. 45 (2012) 317–326, https://doi.org/10.1021/ar200113c.
[46] J.N. Israelachvili, Intermolecular and Surface Forces, 3rd ed., Academic Press, Amsterdam, 2011 doi:10.1016/B978-0-12-375182-9.10025-9.
[47] D.J. Shaw, Introduction to Colloid & Surface Chemistry, 4th ed., Butterworth Heinemann, Oxford, 1992.
[48] B. Jachimska, M. Wasilewska, Z. Adamczyk, Characterization of globular protein solutions by dynamic light scattering, electrophoretic mobility, and viscosity measurements, Langmuir. 24 (2008) 6866–6872.
[49] M. Boström, D.F. Parsons, A. Salis, B.W. Ninham, M. Monduzzi, Possible origin of the inverse and direct Hofmeister series for lysozyme at low and high salt concentrations, Langmuir. 27 (2011) 9504–9511, https://doi.org/10.1021/la202023r.
[50] D.F. Parsons, C. Carucci, A. Salis, Buffer-specific effects arise from ionic dispersion forces, Phys. Chem. Chem. Phys. 24 (2022) 6544–6551, https://doi.org/10.1039/D2CP00223J.
[51] O. Matsarskaia, F. Roosen-Runge, F. Schreiber, Multivalent ions and biomolecules: attempting a comprehensive perspective, ChemPhysChem. 21 (2020) 1742–1767, https://doi.org/10.1002/cphc.202000162.
[52] D.F. Parsons, A. Salis, The impact of the competitive adsorption of ions at surface sites on surface free energies and surface forces, J. Chem. Phys. 142 (2015) 134707, https://doi.org/10.1063/1.4916519.
[53] C.M.H. Ferreira, I.S.S. Pinto, E.V. Soares, H.M.V.M. Soares, (Un)suitability of the use of pH buffers in biological, biochemical and environmental studies and their interaction with metal ions-a review, RSC Adv. 5 (2015) 30989–31003, https://doi.org/10.1039/c4ra15453c.
[54] S.O. Ugwu, S.P. Apte, The effect of buffers on protein conformational stability, Pharm. Technol. 86–113 (2004).